

Hepatic Vasculopathy and Regenerative Responses of the Liver in Fatal Cases of COVID-19



Barbara Kaltschmidt,* Antonia D. E. Fitzek,[‡] Julia Schaedler,[‡] Christine Förster,[§] Christian Kaltschmidt,* Torsten Hansen,^{||} Fabian Steinfurth,[¶] Beatrice A. Windmüller,* Christian Pilger,[#] Cihang Kong,[#] Kashika Singh,[¶] Axel Nierhaus,** Dominic Wichmann,** Jan Sperhake,[‡] Klaus Püschel,[‡] Thomas Huser,[#] Martin Krüger,^{‡‡} Simon C. Robson,^{§§} Ludwig Wilkens,[§] and Jan Schulte am Esch[¶]

*Department of Cell Biology, Faculty of Biology, University of Bielefeld, Bielefeld, Germany; †Department of Legal Medicine, University Medical Center Hamburg-Eppendorf, Hamburg, Germany; ‡Institute of Pathology, KRH Hospital Nordstadt, affiliated with the University Hospital of the University of Bielefeld, Campus Bielefeld-Bethel, Hannover, Germany; §Institute of Pathology, University Hospital OWL of the University of Bielefeld, Campus Klinikum Lippe, Detmold, Germany; ¶Department of General and Visceral Surgery, University Hospital OWL of the University of Bielefeld, Campus Bielefeld-Bethel, Bielefeld, Germany; #Biomolecular Photonics, Faculty of Physics, University of Bielefeld, Bielefeld, Germany; **Department of Intensive Care Medicine, University Medical Center Hamburg-Eppendorf, Hamburg, Germany; ‡‡Department of Internal Medicine and Gastroenterology, University Hospital OWL of the University of Bielefeld, Campus Bielefeld-Bethel, Bielefeld, Germany; and §§Center for Inflammation Research, Department of Anesthesia and Division of Gastroenterology, Department of Medicine, Beth Israel Deaconess Medical Center, Harvard Medical School, Boston, Massachusetts

Severe acute respiratory syndrome coronavirus-2 (SARS-CoV-2) infects the nasopharynx and lungs and causes coronavirus disease-2019 (COVID-19). It may impact the heart, brain, kidney, and liver.¹ Although functional impairment of the liver has been correlated with worse clinical outcomes, little is known about the pathophysiology of hepatic injury and repair in COVID-19.^{2,3} Histologic evaluation has been limited to small numbers of COVID-19 cases with no control subjects^{2,4} and demonstrated largely heterogeneous patterns of pathology.^{2,3}

Methods

Liver tissues of 60 patients who died of COVID-19 pneumonia were obtained from complete autopsies performed in Hamburg between March and June 2020. A cohort of 13 patients with fatal pneumonia in the absence of SARS-CoV-2 infection served as control subjects.

Hematoxylin and eosin staining and immunohistochemistry were applied to comprehensively evaluate the pathophysiology and regeneration aspects at the level of the hepatic microarchitecture. Label-free coherent Raman scattering and second harmonic generation imaging visualized major morphologic changes, revealing steatosis and dilatation of sinusoids.

Results

There were no significant differences in the patient characteristics except for preexisting neurologic conditions ($P = .04$) (Supplementary Table 1). Only 5 patients with COVID-19 and 1 control subject had history of liver

disease. A minority of patients in the COVID-19 group (17%) received intensive care at the time of death with a trend within that group toward home or nursing home care, when compared with control subjects (Supplementary Table 1).

Quantitative real-time polymerase chain reaction and in situ hybridization revealed viral RNA and replicative intermediates in liver tissues. Viral nucleocapsid protein was detected in hepatic stem/progenitor cells (HSPC), cholangiocytes, and hepatocytes (Figure 1A). SARS-CoV-2 was detected at the RNA and/or protein level in 25% of livers in COVID-19 patients (Supplementary Table 1). Quantitative real-time polymerase chain reaction demonstrated 2 out of 5 bile samples positive for SARS-CoV-2 (data not shown).

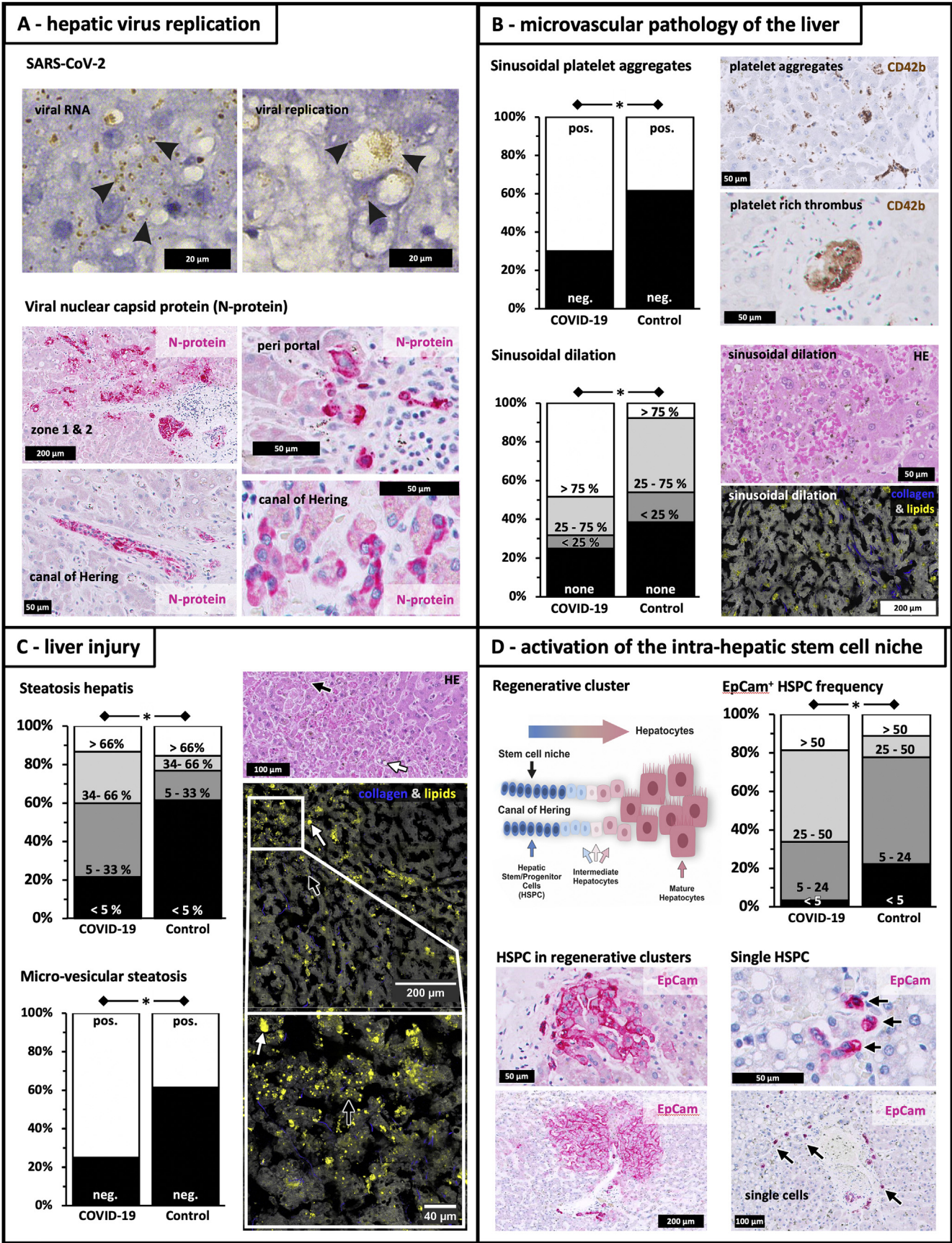
Sinusoidal platelet-aggregates were predominantly observed in the hepatic microvasculature of COVID-19 patients when compared with control subjects (70% vs 30%; $P = .032$) (Figure 1B). Likewise, sinusoidal ($P = .024$) (Figure 1B) and portal dilatation were observed ($P = .002$) (Supplementary Table 1). Hepatic microvascular thrombosis in COVID-19 patients was predominantly observed in nonhospitalized patients (32%; not receiving anticoagulant therapy), when compared with general in-patients (3%) and

Most current article

© 2021 by the AGA Institute. Published by Elsevier, Inc. This is an open access article under the CC BY-NC-ND license (<http://creativecommons.org/licenses/by-nc-nd/4.0/>).

1542-3565

<https://doi.org/10.1016/j.cgh.2021.01.044>



those requiring intensive care (10%; $P = .016$; data not shown).

COVID-19 patients demonstrated more hepatic steatosis ($P = .046$), mainly the microvesicular variant ($P = .01$), when compared with SARS-CoV-2-negative control subjects (Figure 1C). Severe intrahepatic injury was associated with the activation of the intrahepatic stem cell niche along the canal of Hering (Figure 1D), resulting in regenerative clusters of EpCAM⁺HSPC, hepatobiliary intermediate cells, and premature hepatocytes (Figure 1D). Increased numbers of EpCAM⁺HSPC were observed alone, and in regenerative clusters, in patients with COVID-19, when compared with control livers (>25 HSPC/10 field views: 66% vs 22%; $P = .020$) (Figure 1D).

Discussion

We show here secretion of virus into bile and that replication of SARS-CoV-2 occurs in liver tissues during COVID-19. Viral infection of HSPC was observed, comparable with that noted in lung alveolocyte progenitors in the first variant of SARS-CoV infections.⁵

The major pathologic finding is that microvascular changes and platelet-rich thromboembolic phenomena reflect disordered thromboregulation and vascular insults as described previously.^{4,6} As noted with other prothrombotic features of SARS-CoV-2 infections,^{4,7} our observation of microthrombotic pathology predominantly occurring at time of death in nonhospitalized patients suggests that early initiation of anticoagulant therapy in those hospitalized may attenuate microvascular disease of the liver.

Platelet activation, sinusoidal injury, and parenchymal damage result in necrosis, which may be combined with predominantly microvesicular hepatocyte steatosis. Previous reports on postmortem evaluations have demonstrated hepatic steatosis to variable degrees in COVID-19 and seem to demonstrate macrovesicular over microvesicular forms of steatosis.^{3,4}

We demonstrate that vascular injury is accompanied by activation of the intrahepatic stem cell compartment showing features of aberrant regeneration. Similar scenarios of HSPC activation, correlating with the extent of liver cell necrosis, as noted here, have been also shown in hepatitis B-mediated liver injury.⁸

We conclude that SARS-CoV-2 infects the liver as part of systemic illness and results in substantial microvascular thrombotic disease, organ injury, and attempts at regeneration.

Supplementary Material

Note: To access the supplementary material accompanying this article, visit the online version of *Clinical Gastroenterology and Hepatology* at www.cghjournal.org, and at <http://doi.org/10.1016/j.cgh.2021.01.044>.

References

1. Puelles VG, Lutgehetmann M, Lindenmeyer MT, et al. Multi-organ and renal tropism of SARS-CoV-2. *N Engl J Med* 2020; 383:590–592.
2. Lagana SM, Kudose S, Luga AC, et al. Hepatic pathology in patients dying of COVID-19: a series of 40 cases including clinical, histologic, and virologic data. *Mod Pathol* 2020; 33:2147–2155.
3. Saviano A, Wrensch F, Ghany MG, et al. Liver disease and COVID-19: from pathogenesis to clinical care. *Hepatology* 2020: online ahead of print.
4. Rapkiewicz AV, Mai X, Carsons SE, et al. Megakaryocytes and platelet-fibrin thrombi characterize multi-organ thrombosis at autopsy in COVID-19: A case series. *EClinicalMedicine* 2020; 24:100434.
5. Chen Y, Chen VS, Zheng B, et al. A novel subset of putative stem/progenitor CD34+Oct-4+ cells is the major target for SARS coronavirus in human lung. *J Exp Med* 2007; 204:2529–2536.
6. Aid M, Busman-Sahay K, Vidal SJ, et al. Vascular disease and thrombosis in SARS-CoV-2-infected rhesus macaques. *Cell* 2020;183:1354–1366.
7. Ionescu F, Jaiyesimi I, Petrescu I, et al. Association of anti-coagulation dose and survival in hospitalized COVID-19

Figure 1. Microvascular pathology and regenerative responses in livers of COVID-19 patients. SARS-CoV-2 replication, histopathology, and regeneration responses of the liver in fatal COVID-19. (A) Viral replication. SARS-CoV-2 viral RNA (“viral RNA”; +strand, brown dots indicated by black arrows) detected by in situ hybridization and replicative viral intermediates (“viral replication”; -RNA, brown dots indicated by black arrows). Immunohistochemistry shows immunoreactivity against viral nucleocapsid protein (red) in hepatocytes within acinar zones I and II, periportal HSPC, cholangiocytes of portal bile ducts, and premature hepatocytes along the canal of Hering. (B) Microvascular pathology. Sinusoidal platelet aggregates and thrombi (anti-CD42b staining), frequent in COVID-19 patients. Sinusoidal dilatation is noted in hematoxylin and eosin (HE) staining. Coherent Raman scattering microscopy provided label-free contrast for tissue structure (grey) and lipid droplet identification (yellow), whereas second harmonic generation provided contrast for collagen fibers (blue). (C) Liver injury. High levels of hepatocyte steatosis in COVID-19 patients, in comparison with control subjects, as detected by HE staining and coherent Raman scattering/second harmonic generation (lipid droplets in yellow and collagen in blue). White arrows indicate macrovesicular steatosis, whereas black arrows show microvesicular steatosis. (D) Intrahepatic stem cell niche. Drawing of the bipotent intrahepatic stem cell compartment, which is located in the canal of Hering. On severe hepatic injury HSPC emerge and expand, contributing to liver repair. HSPC are detected as single cells (indicated by black arrows) or in regenerative clusters comprised of EpCAM⁺ HSPC, hepatobiliary intermediate cells, and premature hepatocytes, which are adjacent to the canal of Hering. Stem cell marker EpCam (red) is also expressed by numerous HSPC and intermediates of hepatocytes/cholangiocytes and regenerative clusters of periportal hepatocytes of irregular size and shape. HSPC frequency in column diagram represents numbers of HSPC per 10 field views. * $P < .05$.

patients: A retrospective propensity score weighted analysis. *Eur J Haematol* 2021;106:165–174.

8. Nissim O, Melis M, Diaz G, et al. Liver regeneration signature in hepatitis B virus (HBV)-associated acute liver failure identified by gene expression profiling. *PLoS One* 2012;7:e49611.

Reprint requests

Address requests for reprints to: Jan Schulte am Esch, MD, Department of General and Visceral Surgery, Protestant Hospital of Bethel Foundation, University Hospital OWL of the University of Bielefeld, Campus Bielefeld-Bethel, Schildescher Straße 99, 33611 Bielefeld, Germany. e-mail: jan.schulteamesch@evkb.de; fax: +49-521 772-77402.

Acknowledgments

Barbara Kaltschmidt, Antonia D.E. Fitzek, Julia Schaedler, and Christine Förster contributed equally.

Martin Krüger, Simon C. Robson, Ludwig Wilkens, and Jan Schulte am Esch contributed equally.

Conflicts of interest

The authors disclose no conflicts.

Funding

Beatrice A. Windmüller is funded by a grant of the Bethel foundation. Christian Pilger and Cihang Kong were supported by the European Union's Horizon 2020 research and innovation program under the Marie Skłodowska-Curie Grant (Agreement No. 766181, project DeLIVER). Simon C. Robson acknowledges support from Department of Defense Award W81XWH-16-0464.

Supplementary Methods

Autopsies and Liver Sampling

We analyzed liver samples from a cohort of 60 consecutive patients deceased with COVID-19 including cases of none to moderate levels of autolysis. We excluded samples with a high degree of autolysis. Autopsies were carried out by order of the Hamburg health authorities in accordance to the German Infection Protection Act §25 para. 4. The Ethics Committee of the Hamburg Medical Association agreed in principle to this procedure in a vote on April 22, 2020 (file number PV7311, "SARS-CoV-2: Post-mortem description of COVID-19-associated deaths"). The study complied with the tenets of the Declaration of Helsinki. During the autopsies, liver tissue samples were taken and fixed in buffered 4% formaldehyde and virologic swabs were retained. All deceased patients in the COVID-19 group were positive for SARS-CoV-2 viral RNA using a throat smear followed by immediate quantitative real-time polymerase chain reaction (qRT-PCR). A control group was constituted of 13 patients with fatal pneumonia, but absence of SARS-CoV-2 infection.

In Situ Hybridization

Viral RNA and viral replication of SARS-CoV-2 were analyzed in liver sections of patients who died of COVID-19, using RNAscope (ACDbio, Newark, CA). Microphotographs were taken using bright field microscopy.

Quantitative Real-Time Polymerase Chain Reaction

RNA extracted from paraffin sections using the Maxwell RSC (Promega, Madison, WI) was used for RT-PCR analysis (RealStar SARS-CoV-2 RT-PCR Kit 1.0, Altona Diagnostics, Hamburg, Germany).

Histopathology

Standard staining. One tissue block was taken from a representative sampling area of each patient and embedded in paraffin. Three micrometer paraffin sections were stained with hematoxylin and eosin, Elastica van Gieson, periodic acid-Schiff, reticulin stain (Gomori), and iron stain (Perls Prussian blue).

Immunohistochemical staining

Staining was done using Dako Omnis (DAKO, Agilent, Santa Clara, CA) with the following antibodies: anti-CK7, anti-EpCAM, anti-CD31, anti-CD34, anti-CD42b, and anti-SARS-CoV nucleocapsid. Detection was either with DAB or alkaline phosphatase/red. Microphotographs were taken using bright field microscopy.

Nonlinear Optical Microscopy

A custom-built coherent Raman scattering microscope was used to image fixed liver sections. Coherent Raman scattering visualizes lipids in the sample by probing the 2845 cm^{-1} molecular resonance. Second harmonic generation imaging was performed using a home-built fiber-based femtosecond laser. The overlay of coherent Raman scattering and second harmonic generation channels in different look-up tables were done using the open-source software FIJI.

Statistical Analyses

Dichotomic and nominal variables were analyzed applying Pearson chi-square test. Ordinal variables were subjected to Wilcoxon rank sum test (Mann-Whitney) analyses. Statistical significance was taken as P values $< .05$. Stata/SE version 15.1 for Mac software (StataCorp, College Station, TX) was used for statistical analyses.

Supplementary Table 1. Clinical Characteristics and Autopsy Findings in COVID-19 Pneumonia and the Control Patient Group of Fatal Cases of Pneumonia Unrelated to SARS-CoV-2

Classification	COVID-19 negative	COVID-19 positive	P value
	n = 13	n = 60	
	n = 13	n = 60	
Gender			.347
Female	31 (4)	45 (27)	
Male	69 (9)	55 (33)	
Age, y			.422
≤80	54 (7)	42 (25)	
>80	46 (6)	58 (35)	
Liver disease in medical history	8 (1)	8 (5)	.939
Heart disease in medical history	85 (11)	93 (56)	.299
Lung disease in medical history	77 (10)	63 (38)	.349
Neurologic disease in medical history	15 (2)	47 (28)	.038
Renal disease in medical history	46 (6)	33 (20)	.381
Oncologic disease in medical history	8 (1)	22 (13)	.246
Level of care at time of death			.096
Home/nursing home	23 (3)	32 (19)	
Hospital, low care	31 (4)	52 (31)	
Intensive care unit	46 (6)	17 (10)	
Autolysis of hepatic tissue			.171
None	31 (4)	45 (27)	
Little	31 (4)	37 (22)	
Moderate	39 (5)	18 (11)	
Liver tissue: SARS-CoV-2 and/or nucleocapsid-protein	Positive	0 (0)	.043
Sinusoidal platelet aggregates	Present	39 (5)	.031
Sinusoidal ectasia			.024
None	39 (5)	25 (15)	
Focal (<25%)	15 (2)	7 (4)	
Multifocal (25%–75%)	39 (5)	20 (12)	
Diffuse (>75%)	8 (1)	48 (29)	
Portal ectasia			.002
None	8 (1)	3 (2)	
Focal (<25%)	46 (6)	13 (8)	
Multifocal (25%–75%)	31 (4)	25 (15)	
Diffuse (>75%)	15 (2)	5 (3)	
Portal fibrosis			.293
Widen, no septae	53 (7)	72 (43)	
Widen with septae	15 (2)	5 (3)	
Incomplete cirrhosis	31 (4)	22 (13)	
Cirrhosis	0 (0)	2 (1)	

Supplementary Table 1. Continued

	Classification	COVID-19 negative	COVID-19 positive	P value
		n = 13	n = 60	
Confluent necrosis				
	None	85 (11)	66 (38)	.175
	Focal	8 (1)	10 (6)	
	Moderate	0 (0)	5 (3)	
	Frequent	8 (1)	19 (11)	
Apoptosis (cell count per field view)				
	0–1	77 (10)	81 (47)	.838
	2–4	23 (3)	12 (7)	
	>5	0 (0)	7 (4)	
Hepatic steatosis				
	<5%	62 (8)	22 (13)	.046
	5%–33%	15 (2)	38 (23)	
	34%–66%	8 (1)	27 (16)	
	>66%	15 (2)	13 (8)	
Macrovesicular steatosis	Positive	39 (5)	67 (40)	.058
Microvesicular steatosis	Positive	39 (5)	75 (45)	.010
Kupffer cell siderosis				
	None	85 (11)	88 (53)	.771
	Little	15 (2)	7 (4)	
	Moderate	0 (0)	3 (2)	
	Severe	0 (0)	2 (1)	
Hepatocyte siderosis				
	None	92 (12)	88 (53)	.720
	Little	0 (0)	8 (5)	
	Moderate	8 (1)	2 (1)	
	Severe	0 (0)	2 (1)	
Ductular reaction (CK7)	Positive	77 (10)	87 (52)	.348
Cholestasis (histologically)	Positive	0 (0)	3 (2)	.793
EpCam ⁺ regenerative cluster	Positive	11 (1)	29 (17)	.262
EpCam ⁺ hepatic stem/progenitor cells (count per 10 field views)				
	<5	22 (2)	3 (2)	.020
	5–24	56 (5)	31 (18)	
	25–50	11 (1)	48 (28)	
	>50	11 (1)	19 (11)	

NOTE. Data given are % (n). P value: bold < .05.